The Active Surface Species Ruling Product Selectivity in Photocatalytic CO_2 Reduction over Pt- or Co-promoted TiO_2

*Marta Borges Ordoño and Atsushi Urakawa**

Institute of Chemical Research of Catalonia (ICIQ), The Barcelona Institute of Science and Technology, 16 Av. Països Catalans, 43007 Tarragona, Spain

AUTHOR INFORMATION

Corresponding Author

*E-mail address: aurakawa@iciq.es

ABSTRACT

TiO_2 is an active material for photocatalytic CO_2 reduction. Its performance is improved by the addition of metal or metal oxide as co-catalyst. The enhanced electron-trapping capability is widely attributed to the function of these co-catalysts, but their precise roles are not fully understood. Here, we report how Pt and Co co-catalysts boost formation of H_2 and CH_4 during photocatalytic CO_2 reduction. More specifically, we used in situ diffuse reflectance infrared Fourier transformed spectroscopy (DRIFTS) and multivariate spectral analysis to identify (in)active surface intermediates. The surface formates were identified as the reactive intermediate common to all TiO_2-based catalysts. The catalytic activity and product selectivity are determined by the unique function of the co-catalyst, which distinctly interacts with the TiO_2 surface to produce and decompose formates to H_2 or CH_4. The evolution of the surface species also clarifies the transient nature of photocatalytic activities and how the TiO_2 surface and co-catalysts are deactivated under photocatalytic conditions.

1. INTRODUCTION

The photocatalytic reduction of CO_2 can create opportunities to sustainably convert photon energy to chemical energy via the synthesis of chemical energy carriers such as CH_4 and CH_3OH.[1-2] However, this light-driven conversion is very challenging due to the strong thermodynamic stability of CO_2. First, high energy input is required to activate CO_2, as is evident from the strong reduction potential of -1.9 V (E_{red}^0, vs. RHE) to form a generally well-accepted intermediate, CO_2 radical anion.[3] Another challenge is the presence of protons in photocatalytic reactors to produce hydrocarbon or oxygenate chemicals by reacting with CO_2 and electron. The formation of hydrogen in the proton reduction reaction, which is considered as water reduction in aqueous media, is energetically more favorable ($E_{red}^0 = 0$ V vs. RHE). Consequently, hydrogen production is generally more facile than CO_2 reduction in the photocatalytic conversion of CO_2.[4-5] Therefore, there is a need for photocatalysts that can efficiently harness light while suppressing proton reduction over CO_2 reduction.

In addition to catalyst tuning, engineering approaches such as increased CO_2 pressure[6-8] are effective in improving the performance and product yields of CO_2 reduction. By performing the reaction in gas-phase using gaseous CO_2 and water vapor, it is possible to regulate and limit the amount of water (thus protons) in the system with respect to that of CO_2, thereby creating a favorable environment for CO_2 reduction. At sufficiently high reaction temperatures (above 373 K), this approach could prevent water condensation on the catalyst surface and lead to selective production of carbon-containing chemicals over H_2.[9] Furthermore, in comparison to TiO_2 and TiO_2-based materials (the most actively researched photocatalyst materials), stability is a major issue for photocatalytic CO_2 reduction. This aspect is often neglected in the literature and is not well-understood. Typically, the catalytic activity diminishes gradually over time.[9-10] Causal

explanations for the catalyst deactivation include (i) the loss of surface active sites due to the deposition of carbonaceous species,[9] (ii) changes in the metal oxidation state and/or corrosion,[11-12] and (iii) the decrease of surface OH or defective (active) sites.[13-14] However, there is not yet convincing evidence to elucidate the activation and deactivation processes. This lack of evidence hinders the rational design of photocatalysts for CO_2 reduction.

The most popular and convenient method for improving photocatalysts is to load suitable co-catalyst(s) onto the catalyst to promote electron trapping and facilitate redox reactions of surface chemical species.[15-16] Numerous co-catalysts for TiO_2 have been investigated to target H_2 production and CO_2 reduction.[17-18] As co-catalyst, Pt is reported to greatly enhance CO_2 photoreduction by forming a Schottky-barrier at the Pt-TiO_2 interface.[19-21] However, Pt's high cost has motivated researchers to replace this co-catalyst with other inexpensive and earth-abundant metals. Of these, cobalt (or cobalt oxide) has attracted interest due to its high earth-abundance and visible light adsorption properties.[19-22]

Within this context, we report a mechanistic study of photocatalytic CO_2 reduction over TiO_2. This study elucidates how Pt and Co co-catalysts influence the formation of surface chemical species, and the reaction pathways influencing product selectivity. Surface chemical species and their evolution were studied by in situ diffuse reflectance infrared Fourier transformed spectroscopy (DRIFTS). The interpretations of the spectra were facilitated by multivariate spectral analysis, particularly multivariate curve resolution (MCR). Specifically time-resolved spectra with a high level of band overlaps were disentangled into a set of chemically meaningful pure-component spectra with respective concentration profiles through kinetic resolution without the need for a reference (**Figure S1**).[23-25] The evolutions of surface

chemical species were correlated with comparative catalytic tests to gain insights into how the co-catalysts affected the photocatalytic CO_2 reduction chemistry.

2. METHODOLOGY

Pt/TiO_2 and Co/TiO_2 photocatalysts were prepared by an impregnation method followed by a thermal treatment. First, TiO_2 (P25, Degussa) was calcined at 623 K for 3 h. Then TiO_2 was impregnated with an aqueous solution of $H_2PtCl_6 \cdot xH_2O$ (≥99.99% trace metal basis, Sigma-Aldrich) or $Co(NO_3)_2 \cdot 6H_2O$ (99.999% trace metal basis, Sigma-Aldrich) at 0.2 wt% loading (based on the weight of metal with respect to that of TiO_2). Finally, the prepared materials were calcined at 623 K for 3 h.

Photocatalytic CO_2 reduction activity tests were performed at 423 K to facilitate CO_2 reduction with respect to H_2 formation which is favored at lower temperatures due to higher amount of adsorbed water[9] using a custom-made gas-phase reaction setup consisting of an aluminum cell equipped with a fused silica window. Powdered catalyst (100 mg) was charged at the bottom of the rector. The photocatalyst was treated at 423 K under N_2 at the flow rate of 4.5 mL min^{-1} for 1 h prior to irradiation with a 400 W high-pressure Hg lamp (UV-Technik) without an optical filter. The light source was placed at 8 cm away from the optical port of the reactor. Photocatalytic reaction was performed under CO_2 flow (4.5 mL min^{-1}) saturated with H_2O vapor (water saturator was maintained at 323 K). Repeated and periodical light on/off cycles of 1.5 h duration were used to evaluate catalytic activity. The effluent gas composition was continuously monitored by an online MS (Pfeiffer Vacuum, Omnistar) and microGC (Agilent).

In situ DRIFTS studies were performed on a Vertex 70V FT-IR spectrometer (Bruker) equipped with a liquid nitrogen-cooled MCT detector and a Praying Mantis optical accessory

(Harrick). The optical accessory contained an HVC DRP cell and a combination of optical mirrors to collect and direct the IR light from the sample to the detector. The in situ cell (Harrick) consisted of a sample holder at the center, gas inlet and outlet, heating system, two IR transparent windows made of CaF_2, and a third window made of fused silica for UV irradiation. A few mg of a powder catalyst were loaded into the sample holder of the DRIFTS cell and the sample temperature was set at 423 K under He flow at 4.5 mL min^{-1}. Prior to admission of gaseous CO_2 and H_2O to the cell, the catalyst was first treated under He for 1 h at 423 K, then the atmosphere was switched to water-saturated CO_2 at 4.5 mL min^{-1} when periodic light off/on cycles of 1 h duration each were initiated (Dark1→UV1→Dark2→UV2). All measurements were performed isothermally at 423 K. A SwiftCure PLU-10 UV curing setup (UV-Consulting Peschl) equipped with a high-pressure Hg lamp (250 W) and a quartz optical fiber (3 mm core) was used as the light source for the in situ DRIFTS study. The UV light was guided to the sample through the optical fiber. IR spectra were acquired repeatedly for 60 s at the spectral resolution of 4 cm^{-1}. The spectrum recorded under He right before switching to the flow of water-saturated CO_2 was used as the background.

The obtained time-resolved DRIFT spectra were processed mathematically by multivariate spectral analysis, particularly by MCR, uniquely allowing the extraction of the kinetically pure spectra of surface chemical species and corresponding concentration profiles (expressed in light absorbance). In this work, MCR was performed on a complete series of acquired spectra, that is, under (i) He (light off) and then under gaseous CO_2+H_2O with (ii) light off (Dark1), (iii) light on (UV1), (iv) light off (Dark2) and (v) light on (UV2). Non-negativity constraints were applied for the analysis.

3. RESULTS AND DISCUSSION

3.1. Photocatalytic CO_2 reduction by TiO_2, Co/TiO_2 and Pt/TiO_2. CH_4 and H_2 were the only detectable products of photocatalytic reduction of CO_2 over TiO_2, Co/TiO_2, and Pt/TiO_2 in the presence of water vapor under the continuous flow condition. The amounts and evolution profiles of these products were distinctly different for each catalyst (**Figure 1** and **Table S1** in the Supporting information (SI)). If the formation rates of CH_4 and H_2 were constant, one would expect to observe a straight line for the product concentrations under the flow condition. In reality, a maximum in the concentration of CH_4/H_2 was observed after 15-20 min. It then decayed rapidly until it reached a steady value. Notably, this steady value was observed for H_2 production over TiO_2 (e.g. **Figure 1-a'**). The former activity is termed *transient* activity, indicating deactivation due to a non-regenerative consumption of active surface species such as adsorbed formates and bicarbonates or an irreversible change of the metal oxidation state under UV irradiation. The latter activity is termed *steady state* activity, indicating stable photocatalytic activity, which is likely induced by the semiconducting nature (i.e. the stable charge separation) of catalyst materials. CH_4 could be formed at this high reaction temperature (423 K). The photocatalytic activity for both CH_4 and H_2 production was apparently dominated by transient activity, in agreement with previous reports.[9]

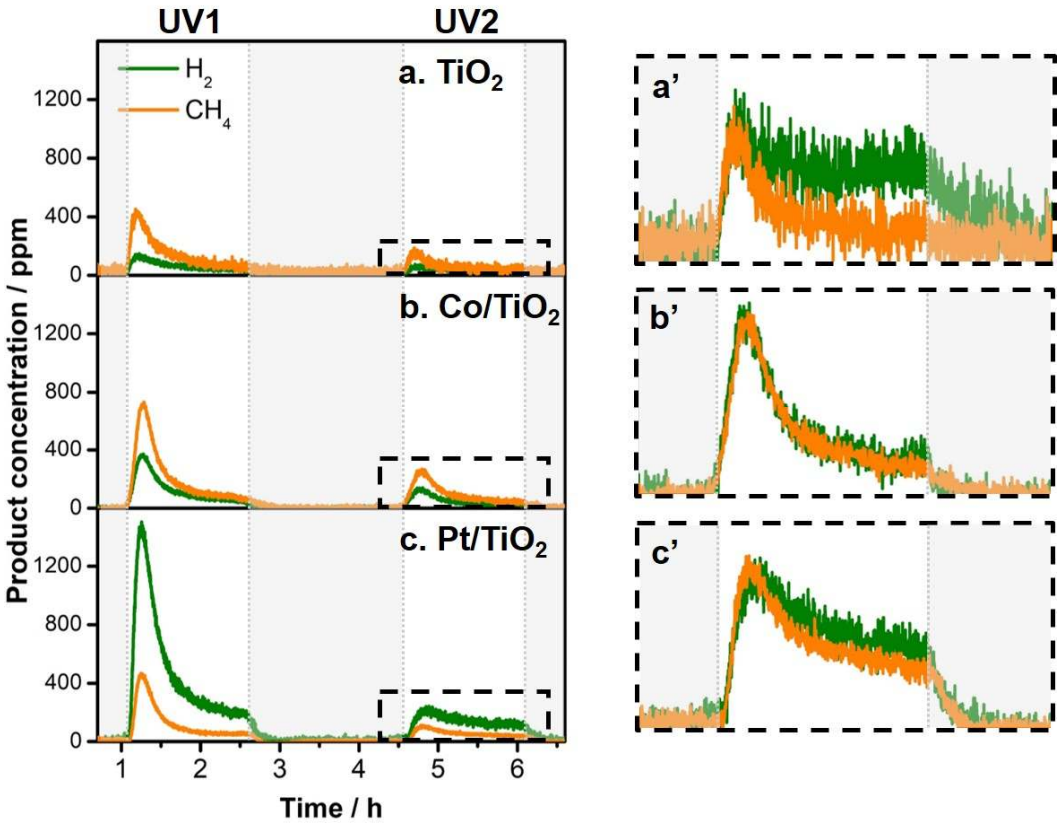

Figure 1. (left) Concentration profiles of CH_4 (orange) and H_2 (green) during photocatalytic CO_2 reduction at 423 K under two UV irradiation cycles (UV1 and UV2) of 1.5 h duration over a) TiO_2, b) Co/TiO_2, and c) Pt/TiO_2. (right) Normalized concentration profiles of CH_4 (orange) and H_2 (green) to the maximum concentration during UV2 for TiO_2 (a'), Co/TiO_2 (b'), and Pt/TiO_2 (c').

The results clarify notable differences in the selectivity trend and amount of products for TiO_2 or Co/TiO_2 against Pt/TiO_2. TiO_2 (**Figure 1-a**) was more selective for CH_4 production. A similar selectivity trend was confirmed for Co/TiO_2 (**Figure 1-b**), with the addition of the Co co-catalyst boosting production of both CH_4 and H_2 by 44% (2.58 μmol g_{cat}^{-1} h^{-1}) and 90% (1.52 μmol g_{cat}^{-1} h^{-1}), respectively. In contrast, the selectivity trend of Pt/TiO_2 (**Figure 1-c**) was reversed with productivity of H_2 (5.28 μmol g_{cat}^{-1} h^{-1}) being remarkably higher than that of CH_4 (1.46 μmol g_{cat}^{-1} h^{-1}).[9, 17] One study of Co/TiO_2 with visible light reported that H_2 was evolved

but CH_4 was not detected,[22] hinting that excitation light wavelength might affect product selectivity.

The major transient activities for CH_4 and H_2 production were recovered to only a minor extent after the dark period. Hence, the subsequent irradiation cycle (UV2) showed poorer catalytic performance. This could indicate deactivation of the photocatalysts, or continuous depletion or ineffective regeneration of active species after light irradiation (**Figure 1** and **Figure S4**).[9, 11, 13-14] The characterization of Pt/TiO_2 after the reaction showed clear changes of the color, Pt particles agglomeration and consequently light adsorption spectra (**Figures S2** and **S3**), indicating the occurrence of irreversible changes of the structure and/or electronic states likely contributing to the catalyst deactivation.

Looking more closely at the CH_4 and H_2 concentration profiles of the three catalysts, the evolution of the two gases was almost identical for Co/TiO_2 and Pt/TiO_2, when the profiles were normalized to the maximum values (**Figure 1-b'** and **1-c'** during UV2; the same conclusion can be drawn from the concentration profiles in UV1, **Figure S4**). In contrast, for TiO_2, the steady-state activity dominated for H_2 production, while the transient activity was responsible for CH_4 production (**Figure 1-a'**). These results suggest that CH_4 and H_2 evolve from the same or highly linked (i.e. in terms of reaction pathways) surface intermediate species over Co/TiO_2 and Pt/TiO_2, whereas two different reaction pathways are active for the formation of CH_4 and H_2 over TiO_2. The former likely occurs through an irreversible consumption of surface intermediate species. The latter likely occurs through the common pathway with separated charges over the semiconducting TiO_2 surface.[20]

3.2. Mechanistic study of photocatalytic CO_2 reduction by in situ DRIFTS. To shed light on the origin of the catalytic activities, reactive surface intermediates, and determining

factors of product selectivity, we performed in situ DRIFTS studies for the three catalysts, mimicking the condition of the catalytic tests (**Figure 1**). The formation of H_2 and CH_4 could not be confirmed due to the small amount of the catalysts used and thus the detection limit. Nevertheless, the evolutions of surface chemical species identified by in situ DRIFTS were in line with those observed in the catalytic tests as discussed below; hence the results from the two different experiments are interpreted in a comparable and comparative manner.

3.2.1. Pt/TiO$_2$. To our surprise, remarkable spectral changes were observed for Pt/TiO_2 in the carbonyl stretching region (2040-2160 cm^{-1}), but only very minor changes were detected for TiO_2 and Co/TiO_2 (**Figure S5**). On Pt/TiO_2, three different surface carbonyl species were identified (**Figure 2-a**) with respective characteristic bands: (i) CO on reduced Pt (Pt^0) at 2065 cm^{-1}, (ii) CO on oxidized Pt (Pt^{n+}) at 2084 cm^{-1},[26-28] and (iii) CO bound to Ti^{3+} at 2114 cm^{-1}.[29-30] These three bands emerged and diminished dynamically in response to the atmosphere change and light on/off. Ti^{4+}-CO bands reported at 2180-2200 cm^{-1} were not detected,[31-32] possibly due to its low stability. To the best of our knowledge, this is the first report on the involvement of carbonyl species during photocatalytic CO_2 reduction, and this is enhanced by the Pt co-catalyst.

Upon changing the gas atmosphere from He to water-saturated CO_2 (Dark1) at 423 K, we first observed an increase in the band intensity of CO on Ti^{3+}. This was confirmed in the 2D plot (**Figure 2-a**) and the component concentration profile extracted with the multivariate spectral analysis (**Figure 2-b** region **1**, and **Figure S6-b**, the corresponding component spectrum of CO on Ti^{3+} is presented in **Figure S6-a**). After 15-20 min in Dark1, at the expense of disappearance of this band, new bands of CO on Pt^0 and on Pt^{n+} appeared prominently and mildly, respectively (**Figure 2-a** and **Figure 2-b** region **2**). In a lower frequency region of 1300-1700 cm^{-1}, formate, carbonate, and bicarbonate species were identified (**Figure S7-a**, **Table S2**).[32-35] Along with the

increase of the band of CO on Ti^{3+} (region **1**), there was a remarkable increase for the carbonate bands. When CO on Ti^{3+} disappeared and CO on Pt^0/Pt^{n+} was formed (region **2**), there was a significant decrease in the intensity of the carbonate bands. We note that these chemical transformations were taking place on the catalyst surface without irradiation of UV light. These observations indicate that the TiO_2 surface induces multiple surface chemical transformations as depicted in **Figure 2-c**, regions **1-2**. After the He treatment, the TiO_2 surface was partially reduced and, upon admission of water-saturated CO_2, CO_2 underwent transformation through its surface adsorption mainly as carbonates, leading to dissociation to CO on Ti^{3+}. The subsequent decrease of CO on Ti^{3+} and formation of CO on Pt^{n+} suggest that there are oxidation processes involving the oxygen atom of CO_2 and H_2O, filling the TiO_2 defective sites. This oxidation of TiO_2 causes the adsorbed CO on TiO_2 to migrate to Pt^0, leading to the abundant formation of CO adsorbed on Pt^0 at the end of Dark1.

Subsequently, upon light irradiation (UV1), we observed a sudden and drastic decrease of CO on Pt^0 and the sharp and transient rise of CO on Ti^{3+}. The latter rise suggests a momentary reduction of Ti^{4+} to Ti^{3+} (**Figure 2-b** region **3**), as typically expected from an electron injection or formation of surface vacancies. In a synchronous fashion, the amount of surface formates increased (**Figure 2-b** region **3**). These observations suggest that CO on Pt^0 reacts with surface OH groups, forming formate species (**Figure 2-c** region **3**).[36-37] The assignment of formate species was affirmed by the emergence of the C-H stretching bands (**Figure S8**).[34-35, 38] However, the sharp increase of Pt^{n+}-CO band indicates a concerted redox process of Pt (oxidation) and TiO_2 (reduction) upon irradiation. After this rapid transformation phase (region **3**), there was a gradual decrease in CO on TiO_2 and formate species, accompanied by a steady increase in carbonate species (region **4**).

The major photocatalytic activity of Pt/TiO_2 for CO_2 reduction and H_2O splitting is highly transient, as illustrated in **Figure 1**. The highly linked or identical chemical origin (intermediate) is suggested as the source of CH_4 and H_2 (see above). The observed evolutions of surface chemical species upon light irradiation, especially in region **3** elucidated by DRIFTS, match well with the transient product evolution profiles of the catalytic test. Hence, surface formates are suggested to be the intermediate leading to CH_4 as well as H_2 over Pt/TiO_2. It is well-known that metallic Pt can efficiently catalyze decomposition of formate/formic acid to yield H_2,[27, 39-40] and that formates can also be an intermediate to methane by further reduction.[19, 41-42] The presence of Pt seems to strongly favor or facilitate both the former reaction and the formation of formate species (**Figure 2-c**). This explains why, of the three catalysts for the photocatalytic CO_2 reduction, Pt/TiO_2 showed the highest transient photocatalytic activity and greatest selectivity toward H_2 through decomposition of formate species.

In the catalytic test (**Figure 1**), the transient activity was not restored after the first light on/off cycle, and considerably lower CH_4 and H_2 productivities were found during UV2. The concentration profiles of the surface species elucidated by the DRIFTS study (**Figure 2-b**) showed that the active formate species were not formed during the subsequent dark (Dark2) and irradiation (UV2) phases (**Figure 2-b** regions **5** and **6**). This supports the hypothesis that formate is indeed the active intermediate, and that the catalyst surface is passivated after the first irradiation (UV1). Based on the continuous decrease of CO on Pt^0, irreversible oxidation of Pt is suggested. The TiO_2 surface could still be reduced to create surface vacancies, as indicated by an initial increase of CO on Ti^{3+} during UV2 (region **6**). However, the oxidation of Pt likely plays a more critical role in the inefficient formation of surface formates. As a consequence, the catalyst

surface was more dominated by carbonates over time, and the H_2 and CH_4 productivities could not be restored (**Figure 2-c**).

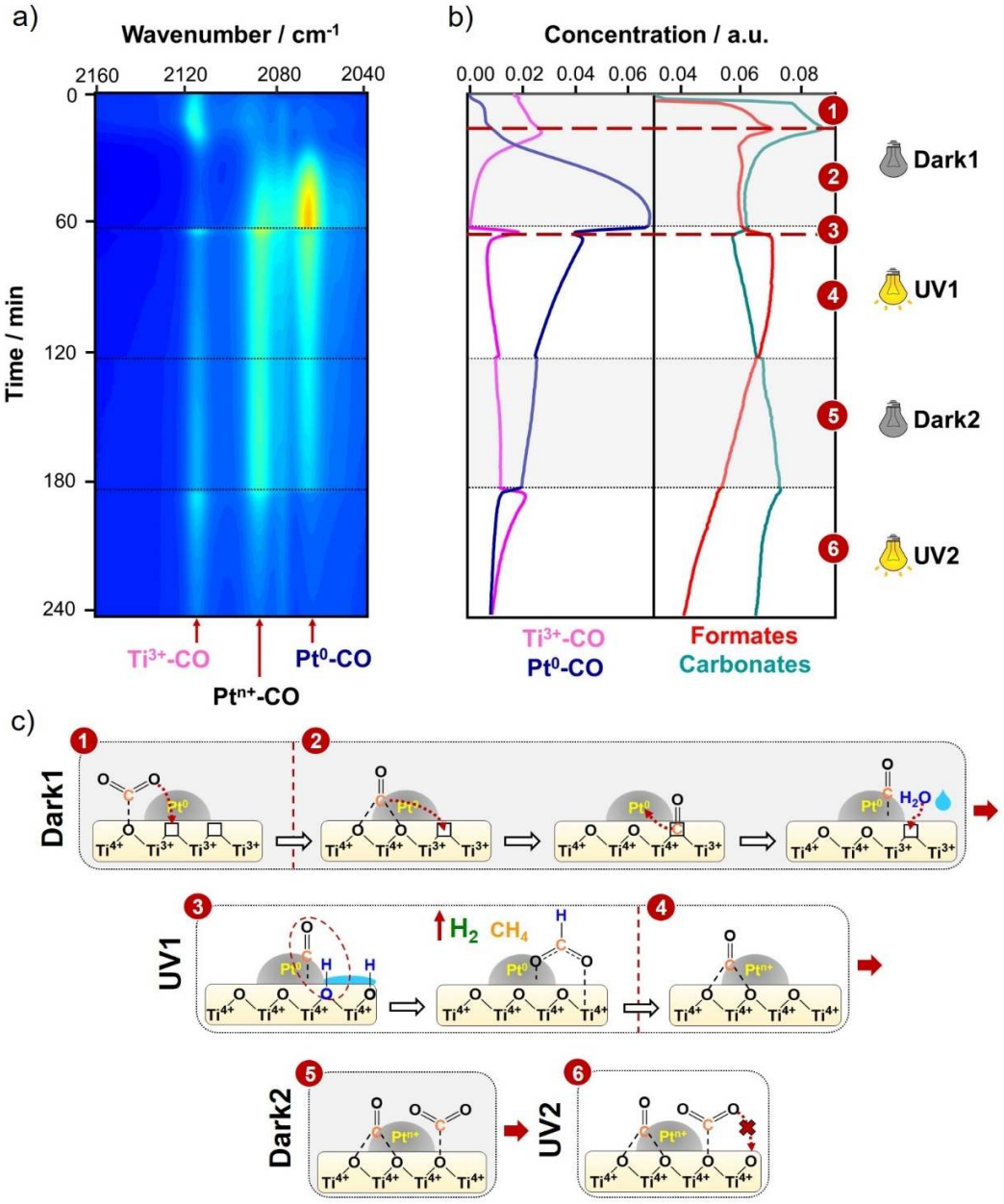

Figure 2. a) Evolution of surface carbonyl species on Pt/TiO_2 with absorbance from -0.02 (blue) to 0.16 (red) under Dark1, UV1, Dark2, and UV2 (top to bottom). b) Component concentration profiles of Ti^{3+}-CO (pink) and Pt^0-CO (blue) obtained by MCR analysis of (a) and of those of

formate (red) and carbonate (cyan) species obtained by MCR analysis of the spectra in the region between 1300-1700 cm^{-1} (component spectra can be found in **Figure S7**). c) Proposed CO_2 reduction mechanism over Pt/TiO_2 (extended in **Figure S9**).

3.2.2. Co/TiO_2 and TiO_2. Comparative in situ DRIFTS studies were performed for Co/TiO_2 and bare TiO_2 in order to understand the origin of the higher CH_4 selectivity of these materials in comparison to Pt/TiO_2, and higher steady-state H_2O splitting activity of TiO_2 (**Figure 1**). As a general trend, both carbonate and bicarbonate species (**Figure S7-b** and **c**) evolved under Dark1 with a notable initial increase (**Figure 3-a** and **3-b** region **1**) followed by a decrease when formate species emerged (region **1**; a different nature of formates on Co/TiO_2 and TiO_2 compared to those on Pt/TiO_2 is suggested in **Figure S7**). In contrast to Pt/TiO_2, there were negligible indications and changes in the region of adsorbed CO (**Figure S5**). This implies that the redox process is less pronounced for TiO_2 and Co than for Pt/TiO_2, suggesting Pt's important role in facilitating the redox surface chemistry of TiO_2. Nevertheless, we expect a certain concentration of defective sites on TiO_2 and, consequently, we assume a similar mechanism as described over Pt/TiO_2 for the formation of (bi)carbonates and reaction of water with TiO_2 surface (**Figure 3**, regions **1** and **2**).

Upon light irradiation (UV1), the concentration of formate species decreased for both Co/TiO_2 (**Figure 3-a** region **3**) and TiO_2 (inset, **Figure 3-b** region **3**), before recovering gradually. This concentration profile was very different to that of Pt/TiO_2 (**Figure 2-b** region **3**), where surface formate species increased rapidly upon irradiation. Nevertheless, the major catalytic activity for CH_4 and H_2 formation was transient (**Figure 1**), and the sudden change in formate species concentration upon irradiation was the indication most linked to transient catalytic activity. Our interpretation is that, for Pt/TiO_2 the formation rate of surface formates is

initially higher than its decomposition rate, while the opposite is true for Co/TiO_2 and TiO_2. This explains the initial consumption of formates upon irradiation in the latter cases. Notably, the presence of Co promoter uniquely enhanced the formation of bicarbonate species (**Figure 3-a** region **3**) under irradiation. This is likely due to the modification of TiO_2 with more basic properties of cobalt oxide.[30, 43] The concentration of surface bicarbonates increases while the concentration of formates decreases. As a result, a fraction of the surface formate species might react with surface water, leading to bicarbonate species. A similar trend of surface species evolution was observed in the second irradiation cycle (UV2). However, as revealed in the catalytic tests, the decrease in formate species was less pronounced during UV2. This supports the idea that surface formates are the origin of the transient catalytic activity.

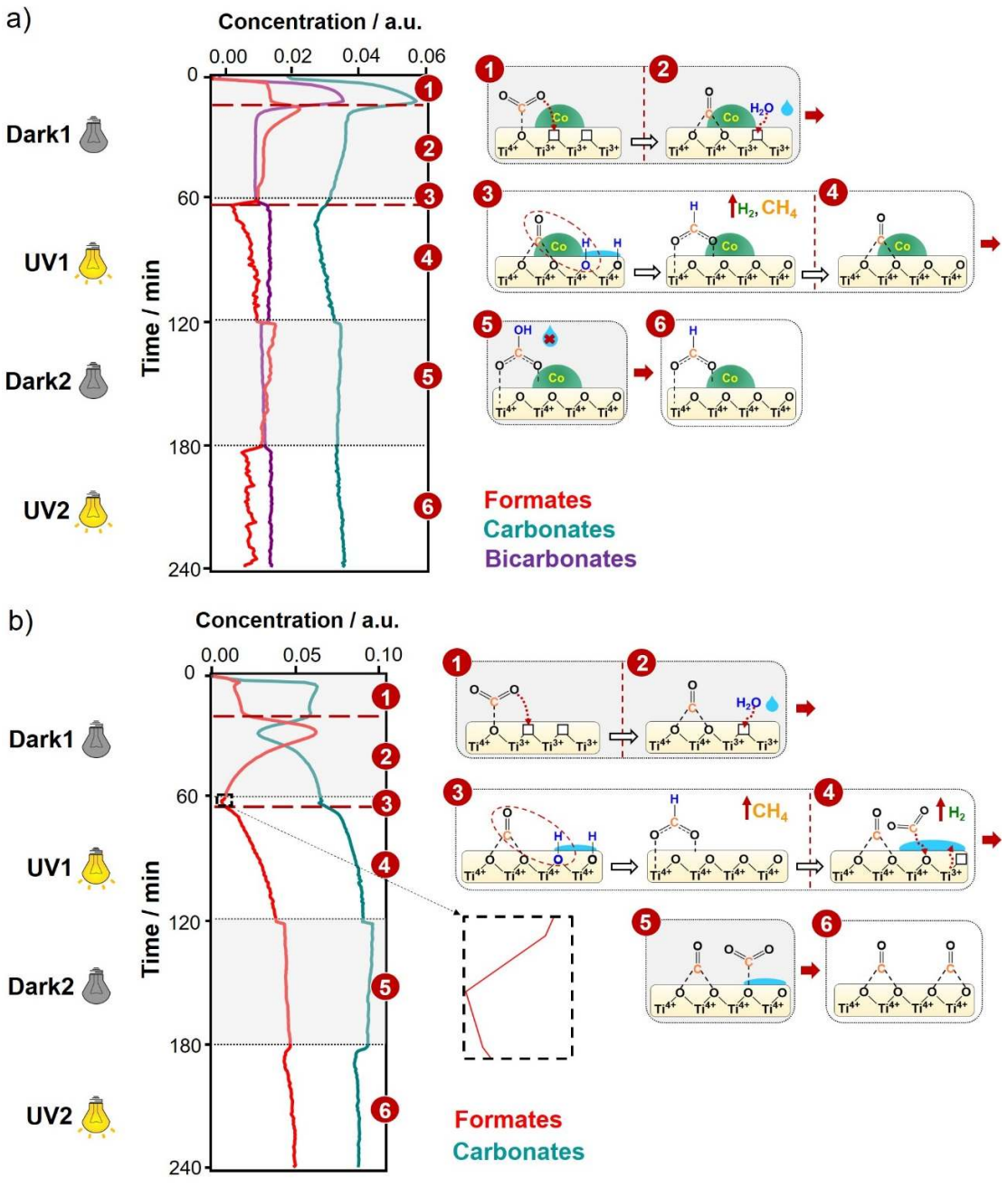

Figure 3. (left) Component concentration profiles of formate (red), carbonate (cyan), and bicarbonate (purple) species obtained by MCR analysis for a) Co/TiO_2 and b) TiO_2 (corresponding component spectra can be found in **Figure S7**). (right) Proposed CO_2 reduction mechanism of Co/TiO_2 (a) and TiO_2 (b).

3.3. Origin of transient activity and deactivation. The above studies show that the transient nature of catalytic activity can be explained by the evolution of surface formates. In the case of Pt/TiO_2, its formation and decomposition, especially to H_2, were facilitated by Pt (**Figure 2**) due to its high activity for formate/formic acid decomposition.[27, 39, 44] In the case of TiO_2 and Co/TiO_2, although surface formates were formed, its decomposition to formates was not facilitated. Rather, its decomposition to CH_4 was favored (Co species were indicated to remain as Co_3O_4 during the reaction, **Figure S10**). The identical transient evolution profiles of CH_4 and H_2 for Pt/TiO_2 and Co/TiO_2 (**Figure 1**) suggest that formates are the common intermediate for their formation.

However, as remarked in **Figure 1**, TiO_2 showed comparably higher steady-state activity for water splitting, while the steady-state activity was virtually absent for Co/TiO_2 despite the similar photocatalytic activity and selectivity trend of Co/TiO_2 and TiO_2 (**Figure 1**). The in situ DRIFTS studies (**Figure 3**) clarified that the major difference between the two is the presence of bicarbonate surface species for Co/TiO_2, while carbonate species are more dominant for TiO_2 under photocatalytic conditions. In addition, for Pt/TiO_2, the oxidation of Pt also greatly contributes to a deterioration in the photocatalytic performance (see above). Due to the undetected gaseous oxygen, there is a possibility that the observed chemical process is not catalytic (e.g. through sacrificial oxidation of Pt). However, by simply comparing the amount of formed CH_4 and oxygen atoms required to oxidize Pt in Pt/TiO_2, the former is two orders of magnitude higher in moles, suggesting that the main product formation processes are catalytic. Bicarbonate is a protonated form of carbonate. Its formation should be facilitated by the presence of surface water. The absence of water splitting activity of Co/TiO_2 suggests that water molecules cannot reach the TiO_2 surface because of its reaction with carbonates to form

bicarbonates, which block the surface sites of TiO_2 (**Figure 3-a** region **5**). On the other hand, carbonates are the dominant surface species on TiO_2 and bicarbonate formation is not facilitated. Thus, when carbonates do not fully cover the TiO_2 surface, water molecules can meet the active sites of TiO_2 under irradiation and H_2 can be produced (**Figure 3-b** region **4**).

In all cases, a gradual increase of carbonate species was observed with time over light on/off cycles. Surface site-blocking by the carbonates was indicated as the main cause of photocatalyst deactivation. Raman spectroscopic characterization of the catalysts before and after the reactions indicated the blockage of surface sites and consequent changes of surface chemical states. Specifically, an increase in fluorescence signals was observed after the reaction (**Figure S11**) due to accumulation of carbonaceous species.[45-46] CH_4 and H_2 productivities were boosted by the addition of methanol to reactivate/enhance catalytic activity[13] (**Figure S12**). An in situ DRIFTS study was conducted under the mimicking reaction condition in the additional presence of methanol. The study demonstrates that carbonate species can be decomposed/transformed (**Figure S13**). It suggests that methanol acts both by reactivating the surface through surface carbonate cleaning and by facilitating formation of formates through oxidation.[47]

4. CONCLUSIONS

Pt and Co co-catalysts uniquely impact on the activity and product selectivity of TiO_2 in the photocatalytic CO_2 reduction. Their unique roles are elucidated by in situ DRIFTS through temporal evolutions of surface species dynamically evolving during light on/off cycles. Decomposition of surface formate species is attributed to the origin of the transient photocatalytic activity. The high selectivity to H_2 of Pt/TiO_2 compared to Co/TiO_2 and TiO_2 is explained by the function of formate/formic acid decomposition facilitated by Pt. Co/TiO_2 and TiO_2 show similar product selectivities, although steady-state H_2 production is only observed for

TiO_2 due to the blocking of surface sites, i.e. disabled access of water to the active sites, by bicarbonate formation on Co/TiO_2. Increased carbonate formation over the catalyst surface is identified as the major cause of surface site blocking, explaining the gradual deactivation of photocatalysts. These insights demonstrate that photocatalytic CO_2 reduction over TiO_2-based materials is driven by a surface-species mediated process. Photocatalyst design strategies should be adapted accordingly, optimizing not only the characteristics of light absorption and electron transfer but also surface chemistry induced by the metal oxide materials as well as co-catalyst.

ASSOCIATED CONTENT

Supporting Information

Photocatalytic activity of TiO_2, Co/TiO_2, and Pt/TiO_2 in CO_2 photocatalytic reduction; UV-Vis DR spectra of TiO_2, Pt/TiO_2, and Co/TiO_2; STEM images of 0.2 wt% Pt and Co before and after reaction; normalized concentration profiles of CH_4 and H_2; comparison of time-resolved DRIFT spectra in the CO stretching region for TiO_2, Co/TiO_2, and Pt/TiO_2; MCR analysis of the spectra in the CO and CH stretching region for Pt/TiO_2; DRIFT spectra and concentration profiles of all the surface species obtained by MCR for Pt/TiO_2, Co/TiO_2, and TiO_2; Raman spectra of Co/TiO_2 before and after the reaction; CH_4 and H_2 concentration profiles of CO_2 reduction with water/methanol vapor; in situ DRIFT spectra in the presence of methanol vapor for TiO_2.

AUTHOR INFORMATION

Corresponding Author

*E-mail address: aurakawa@iciq.es

ORCID

Marta Borges: 0000-0003-1122-1653

Atsushi Urakawa: 0000-0001-7778-4008

Notes

The authors declare no competing financial interest.

ACKNOWLEDGMENTS

The financial support of the Generalitat de Catalunya through the CERCA Programme and recognition (2017 SGR 1633), the ICIQ foundation and MCIU (CTQ2016-75499-R (AEI/FEDER, UE)) are kindly acknowledged. We are also grateful for financial support from Severo Ochoa Excellence Accreditation 2014-2018 (SEV-2013-0319). We thank Dr. Belén Pérez from Institut Català de Nanociència i Nanotecnologia (ICN2), Barcelona for timely support in STEM measurements.

REFERENCES

1. Nikokavoura, A.; Trapalis, C. Alternative Photocatalysts to TiO_2 for the Photocatalytic Reduction of CO_2. *Appl. Surf. Sci.* **2017**, *391*, 149-174.
2. Wang, W.; Soulis, J.; Yang, Y. J.; Biswas, P. Comparison of CO_2 Photoreduction Systems: A Review. *Aerosol. Air. Qual. Res.* **2014**, *14*, 533-549.
3. Álvarez, A.; Borges, M.; Corral-Pérez, J. J.; Olcina, J. G.; Hu, L.; Cornu, D.; Huang, R.; Stoian, D.; Urakawa, A. CO_2 Activation over Catalytic Surfaces. *ChemPhysChem.* **2017**, *18*, 3135-3141.
4. Dhakshinamoorthy, A.; Navalon, S.; Corma, A.; Garcia, H. Photocatalytic CO_2 Reduction by TiO_2 and Related Titanium Containing Solids. *Energ. Environ. Sci.* **2012**, *5*, 9217-9233.
5. Olivo, A.; Ghedini, E.; Signoretto, M.; Compagnoni, M.; Rossetti, I. Liquid Vs. Gas Phase CO_2 Photoreduction Process: Which Is the Effect of the Reaction Medium? *Energies.* **2017**, *10*, 1394.
6. Galli, F.; Compagnoni, M.; Vitali, D.; Pirola, C.; Bianchi, C. L.; Villa, A.; Prati, L.; Rossetti, I. CO_2 Photoreduction at High Pressure to Both Gas and Liquid Products over Titanium Dioxide. *Appl. Catal. B-Environ.* **2017**, *200*, 386-391.
7. Mizuno, T.; Adachi, K.; Ohta, K.; Saji, A. Effect of CO_2 Pressure on Photocatalytic Reduction of CO_2 Using TiO_2 in Aqueous Solutions. *J. Photoch. Photobio. A.* **1996**, *98*, 87-90.
8. Tseng, I. H.; Chang, W.-C.; Wu, J. C. S. Photoreduction of CO_2 Using Sol–Gel Derived Titania and Titania-Supported Copper Catalysts. *Appl. Catal. B-Environ.* **2002**, *37*, 37-48.
9. Bazzo, A.; Urakawa, A. Origin of Photocatalytic Activity in Continuous Gas Phase CO_2 Reduction over Pt/TiO_2. *ChemSusChem.* **2013**, *6*, 2095-2102.
10. Liu, L.; Zhao, C.; Zhao, H.; Pitts, D.; Li, Y. Porous Microspheres of MgO-Patched TiO_2 for CO_2 Photoreduction with H_2O Vapor: Temperature-Dependent Activity and Stability. *Chem. Commun.* **2013**, *49*, 3664-3666.
11. Li, Y.; Wang, W.-N.; Zhan, Z.; Woo, M.-H.; Wu, C.-Y.; Biswas, P. Photocatalytic Reduction of CO_2 with H_2O on Mesoporous Silica Supported Cu/TiO_2 Catalysts. *Appl. Catal. B-Environ.* **2010**, *100*, 386-392.
12. Litter, M. I.; Navío, J. A. Photocatalytic Properties of Iron-Doped Titania Semiconductors. *J. Photoch. Photobio. A.* **1996**, *98*, 171-181.
13. Liu, L.; Zhao, C.; Miller, J. T.; Li, Y. Mechanistic Study of CO_2 Photoreduction with H_2O on Cu/TiO_2 Nanocomposites by In Situ X-ray Absorption and Infrared Spectroscopies. *J. Phys. Chem. C.* **2017**, *121*, 490-499.
14. Maruo, Y. Y.; Yamada, T.; Tsuda, M. Reactivity of CO_2 and H_2O on TiO_2 Catalysts Studied by Gas Phase FT-IR Method and Deactivation Mechanism. *J. Phys. Conf. Ser.* **2012**, *379*, 012036.
15. Daghrir, R.; Drogui, P.; Robert, D. Modified TiO_2 for Environmental Photocatalytic Applications: A Review. *Ind. Eng. Chem. Res.* **2013**, *52*, 3581-3599.
16. Park, H.; Park, Y.; Kim, W.; Choi, W. Surface Modification of TiO_2 Photocatalyst for Environmental Applications. *J. Photoch. Photobio. C.* **2013**, *15*, 1-20.
17. Indrakanti, V. P.; Kubicki, J. D.; Schobert, H. H. Photoinduced Activation of CO_2 on Ti-Based Heterogeneous Catalysts: Current State, Chemical Physics-Based Insights and Outlook. *Energ. Environ. Sci.* **2009**, *2*, 745-758.

18. Ni, M.; Leung, M. K. H.; Leung, D. Y. C.; Sumathy, K. A Review and Recent Developments in Photocatalytic Water-Splitting Using TiO_2 for Hydrogen Production. *Renew. Sust. Energ. Rev.* **2007**, *11*, 401-425.
19. Habisreutinger, S. N.; Schmidt-Mende, L.; Stolarczyk, J. K. Photocatalytic Reduction of CO_2 on TiO_2 and Other Semiconductors. *Angew. Chem. Int. Edit.* **2013**, *52*, 7372-7408.
20. Linsebigler, A. L.; Lu, G.; Yates, J. T. Photocatalysis on TiO_2 Surfaces: Principles, Mechanisms, and Selected Results. *Chem. Rev.* **1995**, *95*, 735-758.
21. Osterloh, F. E. Inorganic Materials as Catalysts for Photochemical Splitting of Water. *Chem. Mater.* **2008**, *20*, 35-54.
22. Ola, O.; Maroto-Valer, M. M. Transition Metal Oxide Based TiO_2 Nanoparticles for Visible Light Induced CO_2 Photoreduction. *Appl. Catal. A-Gen.* **2015**, *502*, 114-121.
23. Jaumot, J.; de Juan, A.; Tauler, R. MCR-ALS GUI 2.0: New Features and Applications. *Chemometr. Intell. Lab.* **2015**, *140*, 1-12.
24. Monakhova, Y. B.; Astakhov, S. A.; Mushtakova, S. P.; Gribov, L. A. Methods of the Decomposition of Spectra of Various Origin in the Analysis of Complex Mixtures. *J. Anal. Chem.+* **2011**, *66*, 351-362.
25. Voronov, A.; Urakawa, A.; Beek, W. v.; Tsakoumis, N. E.; Emerich, H.; Rønning, M. Multivariate Curve Resolution Applied to In Situ X-ray Absorption Spectroscopy Data: An Efficient Tool for Data Processing and Analysis. *Anal. Chim. Acta.* **2014**, *840*, 20-27.
26. Barshad, Y.; Zhou, X.; Gulari, E. Carbon Monoxide Oxidation under Transient Conditions: A Fourier-Transform Infrared Transmission Spectroscopy Study. *J. Catal.* **1985**, *94*, 128-141.
27. Panagiotopoulou, P.; Christodoulakis, A.; Kondarides, D. I.; Boghosian, S. Particle Size Effects on the Reducibility of Titanium Dioxide and Its Relation to the Water–Gas Shift Activity of Pt/TiO_2 Catalysts. *J. Catal.* **2006**, *240*, 114-125.
28. Stakheev, A. Y.; Shpiro, E. S.; Tkachenko, O. P.; Jaeger, N. I.; Schulz-Ekloff, G. Evidence for Monatomic Platinum Species in H-ZSM-5 from FTIR Spectroscopy of Chemisorbed Co. *J. Catal.* **1997**, *169*, 382-388.
29. Busca, G.; Saussey, H.; Saur, O.; Lavalley, J. C.; Lorenzelli, V. FT-IR Characterization of the Surface Acidity of Different Titanium Dioxide Anatase Preparations. *Appl. Catal.* **1985**, *14*, 245-260.
30. Hadjiivanov, K. I.; Klissurski, D. G. Surface Chemistry of Titania (Anatase) and Titania-Supported Catalysts. *Chem. Soc. Rev.* **1996**, *25*, 61-69.
31. Hadjiivanov, K.; Saur, O.; Lamotte, J.; Lavalley, J.-C. FT-IR Spectroscopic Study of NH_3 and CO Adsorption and Coadsorption on TiO_2 (Anatase). *Zeitschrift für Physikalische Chemie* **1994**, *187*, 281.
32. Liao, L. F.; Lien, C. F.; Shieh, D. L.; Chen, M. T.; Lin, J. L. FTIR Study of Adsorption and Photoassisted Oxygen Isotopic Exchange of Carbon Monoxide, Carbon Dioxide, Carbonate, and Formate on TiO_2. *J. Phys. Chem. B.* **2002**, *106*, 11240-11245.
33. Bianchi, D.; Chafik, T.; Khalfallah, M.; Teichner, S. J. Intermediate Species on Zirconia Supported Methanol Aerogel Catalysts: IV. Adsorption of Carbon Dioxide. *Appl. Catal. A-Gen.* **1994**, *112*, 219-235.
34. Guglielminotti, E. Infrared Study of Syngas Adsorption on Zirconia. *Langmuir.* **1990**, *6*, 1455-1460.
35. Kondo, J.; Abe, H.; Sakata, Y.; Maruya, K.-i.; Domen, K.; Onishi, T. Infrared Studies of Adsorbed Species of H_2, CO and CO_2 over ZrO_2. *J. Chem. Soc. Farad. T. 1.* **1988**, *84*, 511-519.

36. Iida, H.; Igarashi, A. Characterization of a Pt/TiO_2 (Rutile) Catalyst for Water Gas Shift Reaction at Low-Temperature. *Appl. Catal. A-Gen.* **2006**, *298*, 152-160.
37. Panagiotopoulou, P.; Kondarides, D. I. Effects of Alkali Additives on the Physicochemical Characteristics and Chemisorptive Properties of Pt/TiO_2 Catalysts. *J. Catal.* **2008**, *260*, 141-149.
38. Bando, K. K.; Sayama, K.; Kusama, H.; Okabe, K.; Arakawa, H. In-Situ FT-IR Study on CO_2 Hydrogenation over Cu Catalysts Supported on SiO_2, Al_2O_3, and TiO_2. *Appl. Catal. A-Gen.* **1997**, *165*, 391-409.
39. Alexeev, O. S.; Chin, S. Y.; Engelhard, M. H.; Ortiz-Soto, L.; Amiridis, M. D. Effects of Reduction Temperature and Metal−Support Interactions on the Catalytic Activity of Pt/ɣ-Al_2O_3 and Pt/TiO_2 for the Oxidation of CO in the Presence and Absence of H_2. *J. Phys. Chem. B.* **2005**, *109*, 23430-23443.
40. Chen, T.; Wu, G.; Feng, Z.; Hu, G.; Su, W.; Ying, P.; Li, C. In Situ FT-IR Study of Photocatalytic Decomposition of Formic Acid to Hydrogen on Pt/TiO_2 Catalyst. *Chiniese. J. Catal.* **2008**, *29*, 105-107.
41. He, H.; Zapol, P.; Curtiss, L. A. Computational Screening of Dopants for Photocatalytic Two-Electron Reduction of CO_2 on Anatase (101) Surfaces. *Energ. Environ. Sci.* **2012**, *5*, 6196-6205.
42. Tan, S. S.; Zou, L.; Hu, E. Kinetic Modelling for Photosynthesis of Hydrogen and Methane through Catalytic Reduction of Carbon Dioxide with Water Vapour. *Catal. Today* **2008**, *131*, 125-129.
43. Wang, Y.; Zhao, J.; Wang, T.; Li, Y.; Li, X.; Yin, J.; Wang, C. CO_2 Photoreduction with H_2O Vapor on Highly Dispersed CeO_2/TiO_2 Catalysts: Surface Species and Their Reactivity. *J. Catal.* **2016**, *337*, 293-302.
44. Chen, J.; Kubota, J.; Wada, A.; Kondo, J. N.; Domen, K. Sum Frequency Generation Spectroscopic Investigation of TiOx/Pt(111): Surface Active Sites and Reaction Paths Probed by Formate. *J. Phys. Chem. C.* **2008**, *112*, 12477-12485.
45. Cats, K. H.; Weckhuysen, B. M. Combined Operando X-ray Diffraction/Raman Spectroscopy of Catalytic Solids in the Laboratory: The Co/TiO_2 Fischer–Tropsch Synthesis Catalyst Showcase. *ChemCatChem.* **2016**, *8*, 1531-1542.
46. Li, C.; Stair, P. C. Ultraviolet Raman Spectroscopy Characterization of Coke Formation in Zeolites. *Catal. Today* **1997**, *33*, 353-360.
47. Whiting, G. T.; Kondrat, S. A.; Hammond, C.; Dimitratos, N.; He, Q.; Morgan, D. J.; Dummer, N. F.; Bartley, J. K.; Kiely, C. J.; Taylor, S. H., et al. Methyl Formate Formation from Methanol Oxidation Using Supported Gold–Palladium Nanoparticles. *ACS Catal.* **2015**, *5*, 637-644.

TOC GRAPHIC

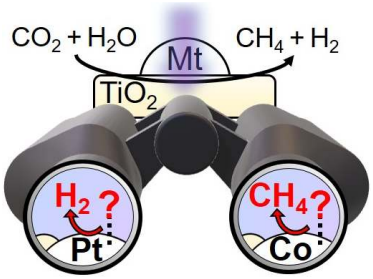

SUPPORTING INFORMATION

Active Surface Species Ruling Product Selectivity in Photocatalytic CO_2 Reduction over Pt- or Co-promoted TiO_2

*Marta Borges Ordoño and Atsushi Urakawa**

Institute of Chemical Research of Catalonia (ICIQ), The Barcelona Institute of Science and Technology, 16 Av. Països Catalans, 43007 Tarragona, Spain

FIGURES AND TABLES

MCR is applied to the raw data spectra matrix (**D**) which contains the spectra recorded with time, then the **D** matrix is decomposed into bilinear contributions of the pure components (columns with concentration (**C**) and spectra profiles (**S**)) obtained by solving the equation $\mathbf{D}=\mathbf{C}\mathbf{S}^{T}+\mathbf{E}$ (Figure S1). Initially, the number of pure components needs to be defined, and then the least square method (MCR-ALS) is used to solve the MCR equation by several iterations until the best combination of **C** and **S** matrices is achieved. This process is repeated until the components with low noise are obtained.[1-3] Spectral components were normalized to the maximum value (set to 1) and the corresponding concentration profiles are scaled accordingly.

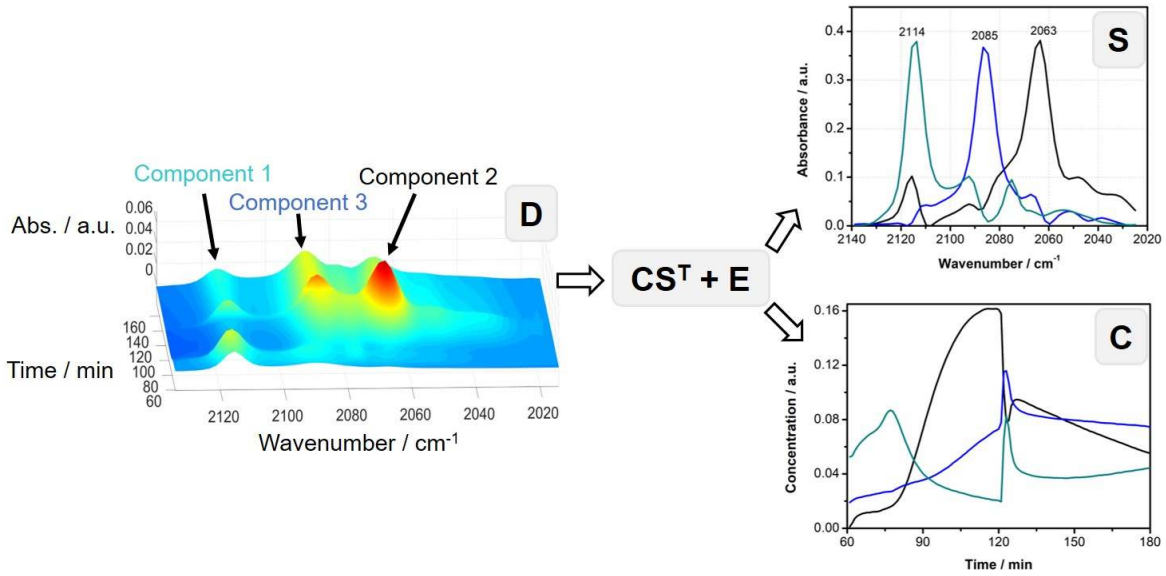

Figure S1. Multivariate curve resolution analysis from DRIFTS data (raw data matrix **D** containing absorbance spectra with time), and the spectral components and their corresponding concentration profiles after performing multivariate analysis on **D**.

Table S1. CH_4 and H_2 productivities obtained from the photoreduction of CO_2 with TiO_2, Pt/TiO_2, and Co/TiO_2. The activity (productivity) was calculated from the concentration profiles for each UV irradiation cycles (e.g. UV1 and UV2). The highest CH_4 and H_2 productivities observed in this work of are highlighted in orange and green, respectively.

	UV	CH_4 ($\mu mol\ g_{cat}^{-1}\ h^{-1}$)	H_2 ($\mu mol\ g_{cat}^{-1}\ h^{-1}$)	CH_4 production respect to TiO_2 (%)	H_2 production respect to TiO_2 (%)
TiO_2	1	1.79	0.80	-	-
	2	0.74	0.51	-	-
Pt/TiO_2	1	1.46	**5.28**	-	560
	2	0.62	1.57	-	208
Co/TiO_2	1	**2.58**	1.52	44	90
	2	1.17	0.62	58	22

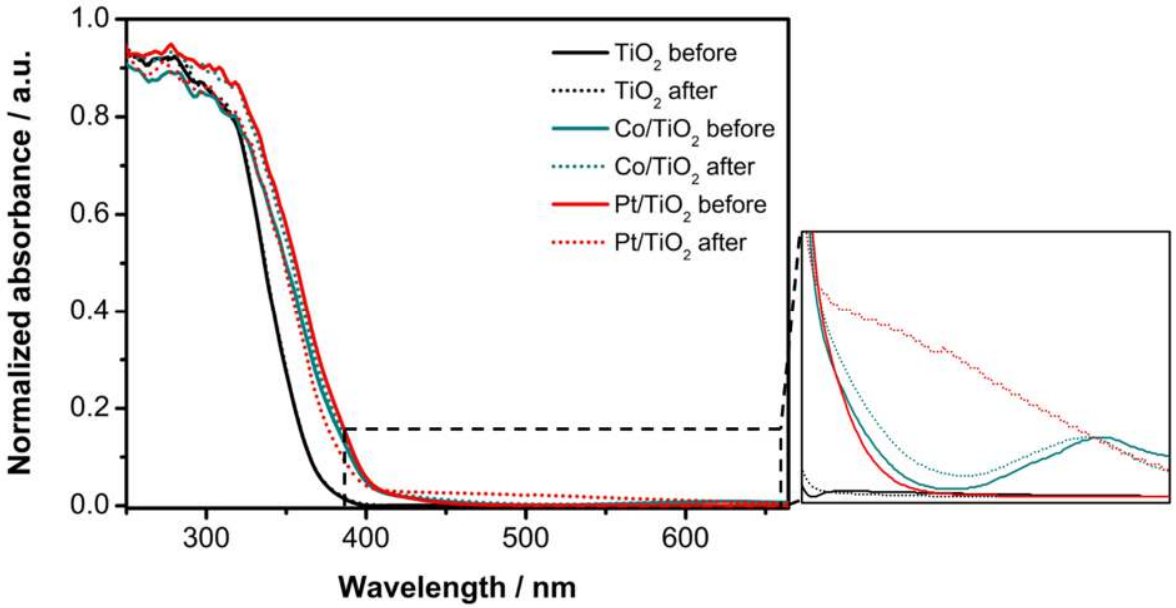

Figure S2. UV-Vis DR spectra of TiO_2 (black), 0.2 wt% Pt/TiO_2 (red), and 0.2 wt% Co/TiO_2 (cyan) before (straight line) and after CO_2 reduction reaction (dotted line). Inset plot shows zoom of the visible light region.

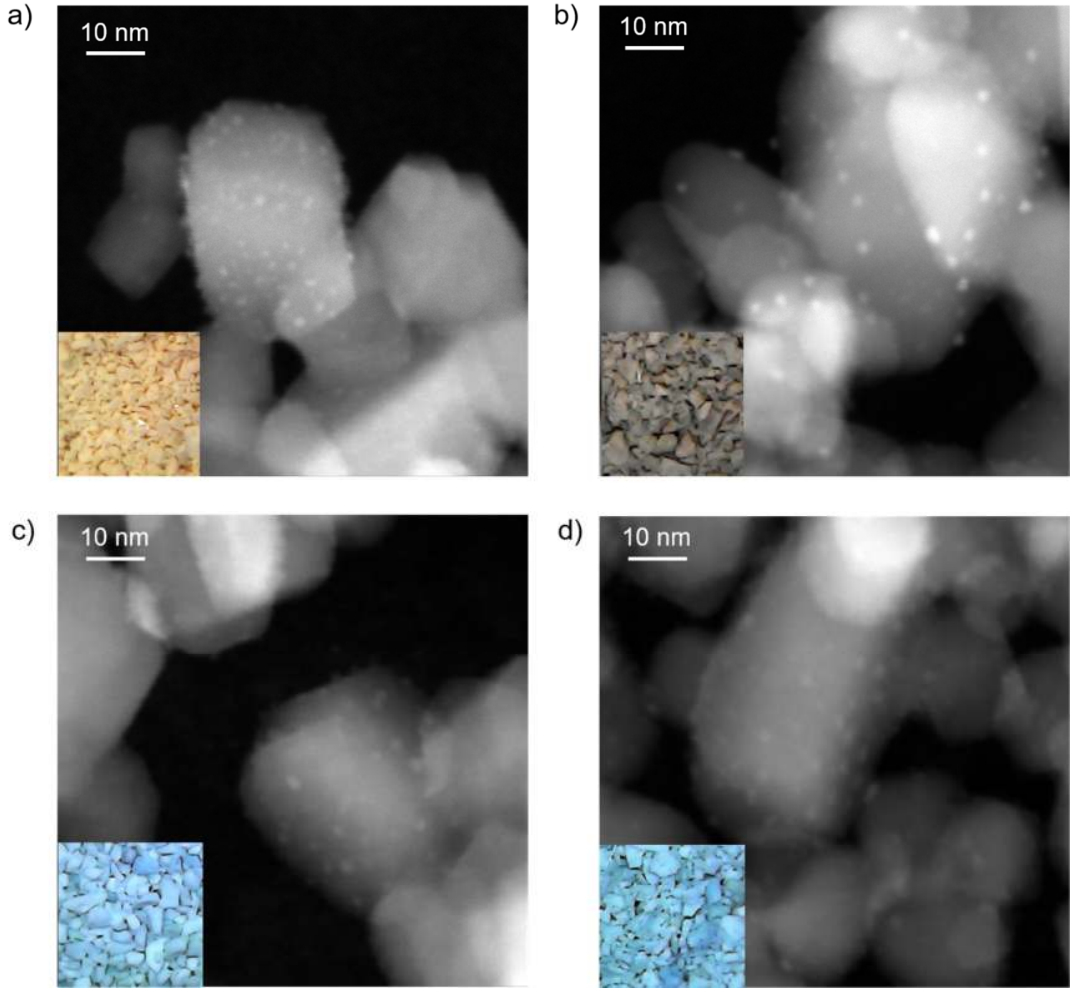

Figure S3. STEM images of 0.2 wt% Pt (**a, b**) and 0.2 wt% Co (**c, d**) on TiO_2 before (**a** and **c**) and after (**b** and **d**) CO_2 photoreduction reaction. The inset pictures correspond with Pt/TiO_2 before (**a**) and after (**b**) reaction, and the corresponding ones of Co/TiO_2 (**c** and **d**). The averaged particle size of Pt-loaded TiO_2 before the reaction was 1.5 nm (**a**), showing a slightly increased size after reaction to 2.2 nm (**b**). The particle size of Co-loaded TiO_2 was retained after reaction with an averaged particle size of 1.8 nm.

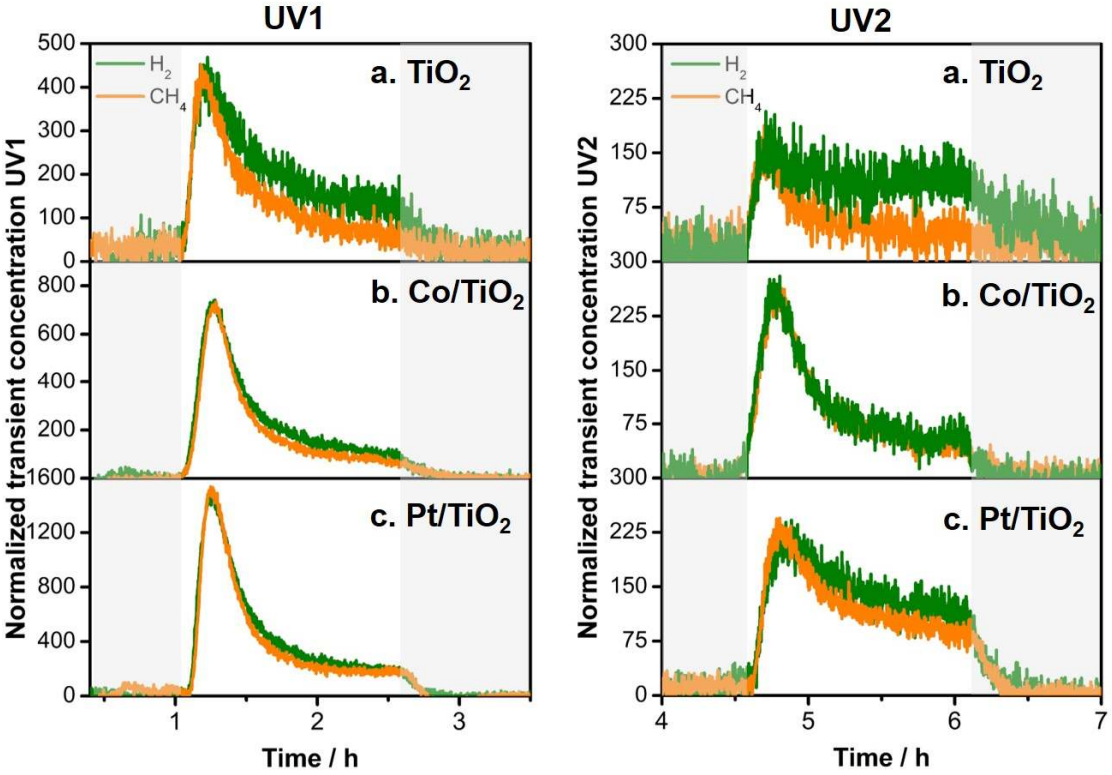

Figure S4. CH_4 (orange) and H_2 (green) concentration profiles normalized by the maximum concentration during UV1 (left) and UV2 (right) for **a**) TiO_2, **b**) Co/TiO_2, and **c**) Pt/TiO_2 in CO_2 photoreduction reaction at 423 K.

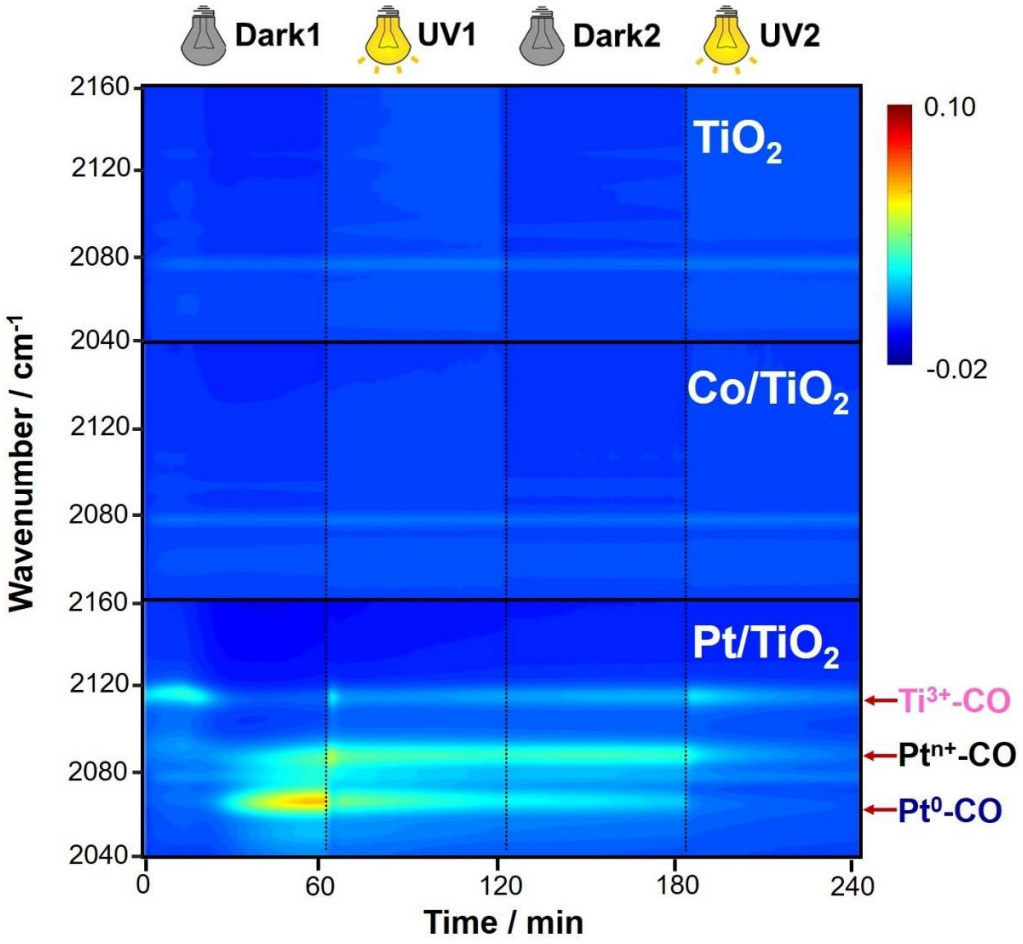

Figure S5. Evolution of carbonyl bands over TiO_2, Co/TiO_2, and Pt/TiO_2 (top to bottom) during CO_2 photoreduction reaction during Dark1, UV1, Dark2, and UV2. Surface carbonyl species on Ti^{3+}, Pt^{n+}, and Pt^0 observed for Pt/TiO_2 to are highlighted. Absorbance ranges from -0.02 (blue) to 0.10 (red).

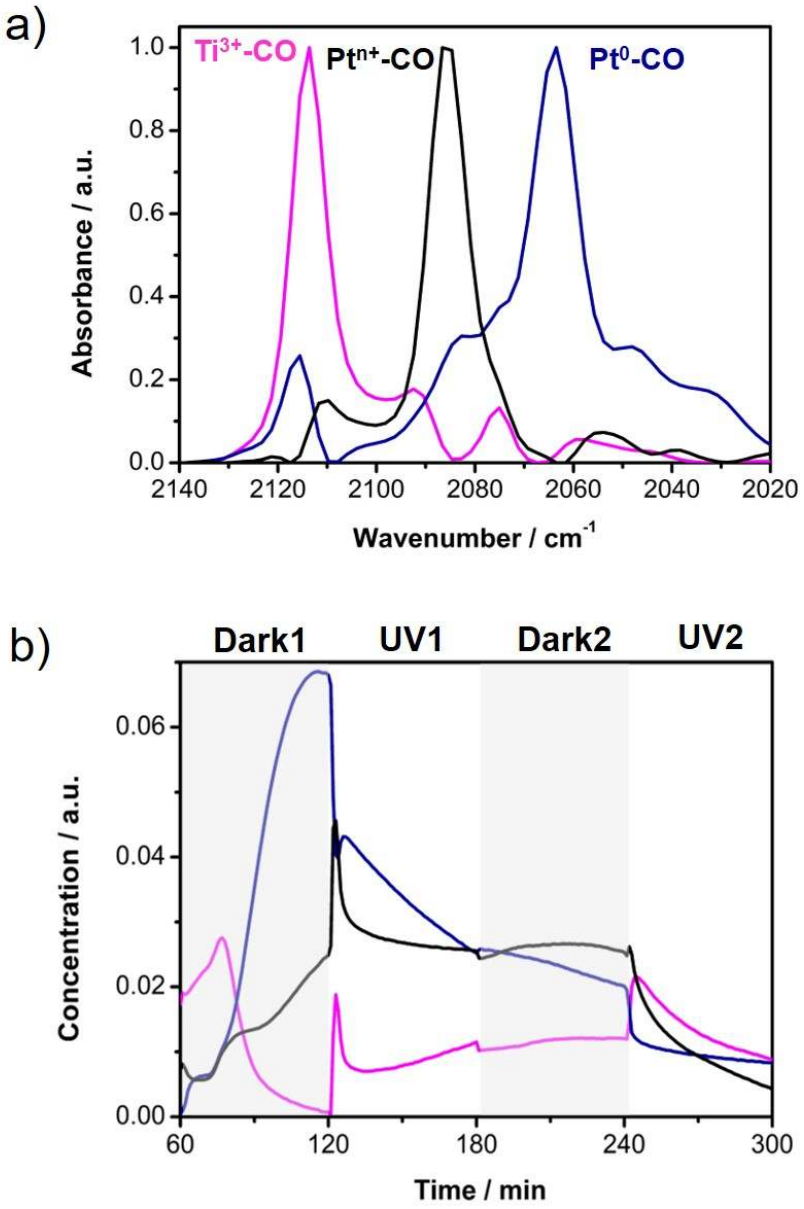

Figure S6. Component spectra (**a**) and concentration profiles (**b**) of the carbonyl species observed over Pt/TiO_2 during CO_2 photoreduction reaction. Three carbonyl species on Pt^0 (blue), oxidized Pt (black), and Ti^{3+} (magenta) are identified.

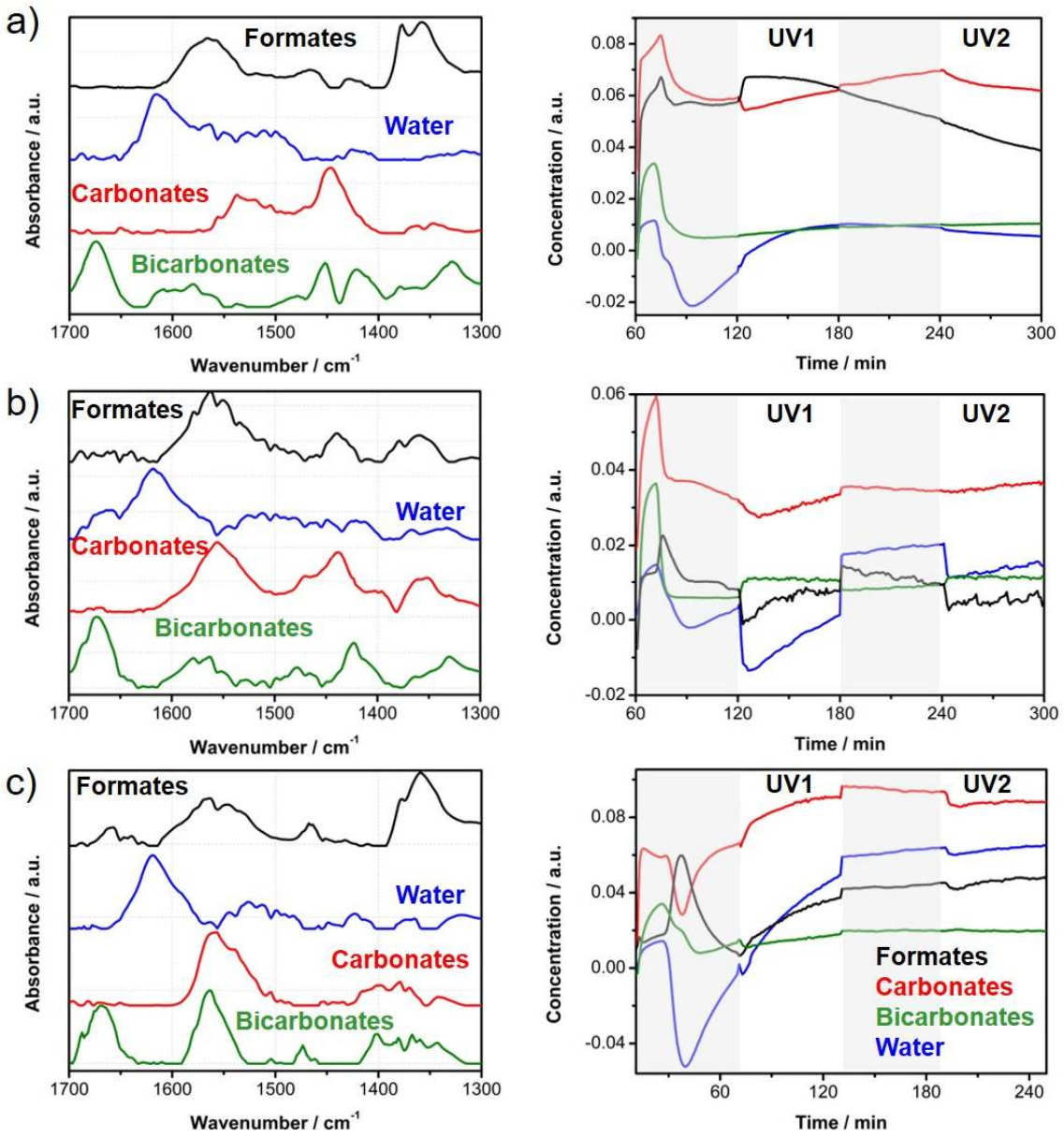

Figure S7. Component spectra and concentration profiles obtained by the MCR analysis of the low frequency region (1300-1700 cm^{-1}) for **a**) Pt/TiO_2, **b**) Co/TiO_2, and **c**) TiO_2. Spectra and concentration profiles are for formates (black), carbonates (red), bicarbonates (green), and water (blue) surface adsorbed species.

Table S2. Comparison between experimental and reported bands used on the assignments of surface chemical species from the component spectra on Figure S7 at low IR frequency region.

Experimental bands (cm^{-1})	Reported bands (cm^{-1})	Attributed to	Reference
1675 and 1450 (Pt) **1672 and 1425 (Co)**	• 1600 and 1470 • 1620 and 1453 • 1673 and 1430	• Bidentate bicarbonates • Bicarbonates • Bicarbonates	• Kondo, J. et al. *J. Chem. Soc. Faraday Trans*., 1988. **84**(2): p. 511-519 • Guglielminotti, E. *Langnmuir*, 1990, **6**(9): p. 1455-1460 • Bando, K. K. et al. *Appl. Catal. A*, 1997,**165**: p. 391-409, Turek, A. et al. *J Phys. Chem*., 1992, **96**(12): p. 5000-5007
1550 and 1340 (Pt) **1560 and 1330 (Co)**	• 1556 and 1325 • 1595 and 1282 • 1579 and 1319 • 1550 and 1310	• Bidentate carbonates • Bidentate carbonates • Bidentate carbonates • Bidentate carbonates	• Bianchi, D. et al. *Appl. Catal. A*, 1994, **112**(2): p. 219-235 • Kondo, J. et al. *J. Chem. Soc. Faraday Trans*., 1988. **84**(2): p. 511-519 • Liao, L.F. et al. *J. Phys. Chem. B*, 2002, **106**(43): p. 11240-11245 • Guglielminotti, E. *Langnmuir*, 1990, **6**(9): p. 1455-1460
1438 (Co) **1440 (Pt)**	• 1483 and 1373 • 1461	• Unidentate carbonates • Monodentate carbonates	• Kondo, J. et al. *J. Chem. Soc. Faraday Trans*., 1988. **84**(2): p. 511-519 • Liao, L.F. et al. *J. Phys. Chem. B*, 2002, **106**(43): p. 11240-11245
1560, 1380, 1360 (Pt) **1560 and 1360 (Co)**	• 2966, 2875, 1586, 1385, 1361 • 1555 and 1370 • 2885-95, 1562, 1370, 1390 • 2933, 2858, 1591, 1353 • 2945, 2921, 2867, 1323	• Formates • Formates • Formates • Formates • Formic acid	• Kondo, J. et al. *J. Chem. Soc. Faraday Trans*., 1988. **84**(2): p. 511-519 • Liao, L.F. et al. *J. Phys. Chem. B*, 2002, **106**(43): p. 11240-11245 • Guglielminotti, E. *Langnmuir*, 1990, **6**(9): p. 1455-1460 • Bando, K. K. et al. *Appl. Catal. A*, 1997,**165**: p. 391-409 • Miller. K.L. et al. *J. Catal*, 2010, **275**(2): p. 294-299

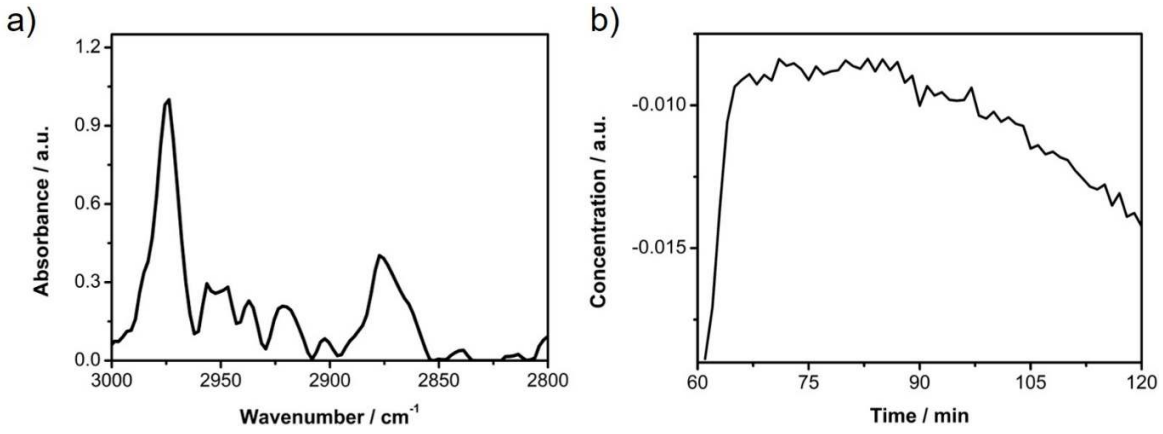

Figure S8. a) Component spectrum and **b**) concentration profile of formate species over Pt/TiO_2 during UV1 obtained by the MCR analysis of the CH region between 2800-3050 cm^{-1}.

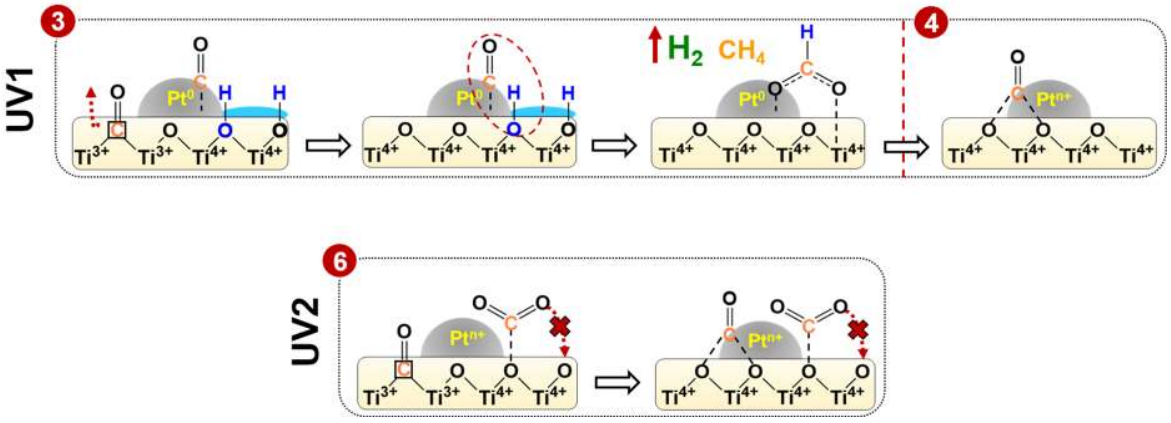

Figure S9. Extended CO_2 reduction mechanism over Pt/TiO_2 from Figure 2-c.

Raman measurements were performed using a BWTEK dispersive i-Raman portable spectrometer equipped with 785 nm excitation laser and a TE-cooled linear array detector. Samples were measured in powder form.

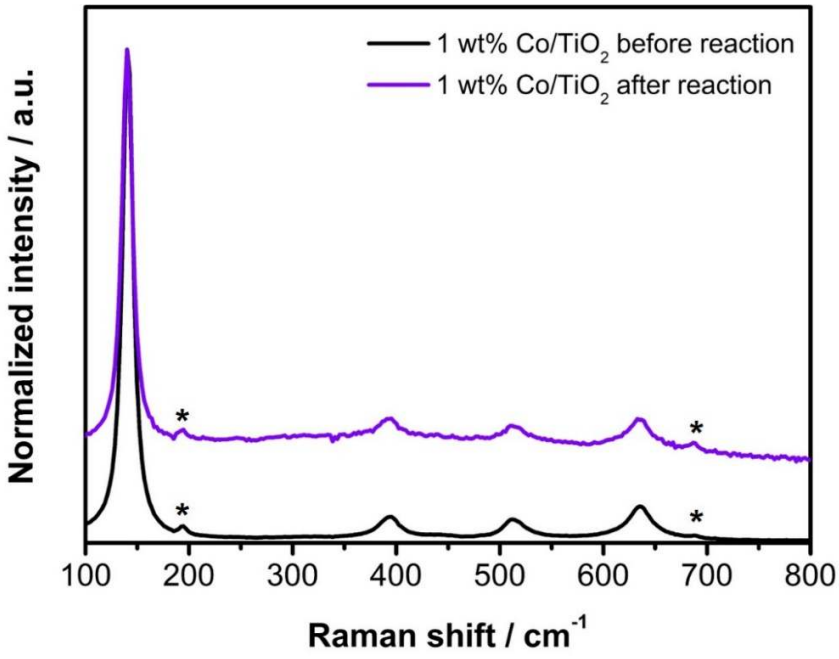

Figure S10. Raman spectra of 1 wt% Co/TiO_2 before and after performing the photocatalytic CO_2 reduction with 785 nm excitation laser (red). 1 wt% Co-loading is shown because for low concentration of cobalt (e.g. 0.2 wt%) signals from Co_3O_4 were not identified. Raman peaks marked with (*) correspond to Co_3O_4 reference material (Jiang, J. and L. Li, *Materials Letters*, 2007. 61(27): p. 4894-4896).

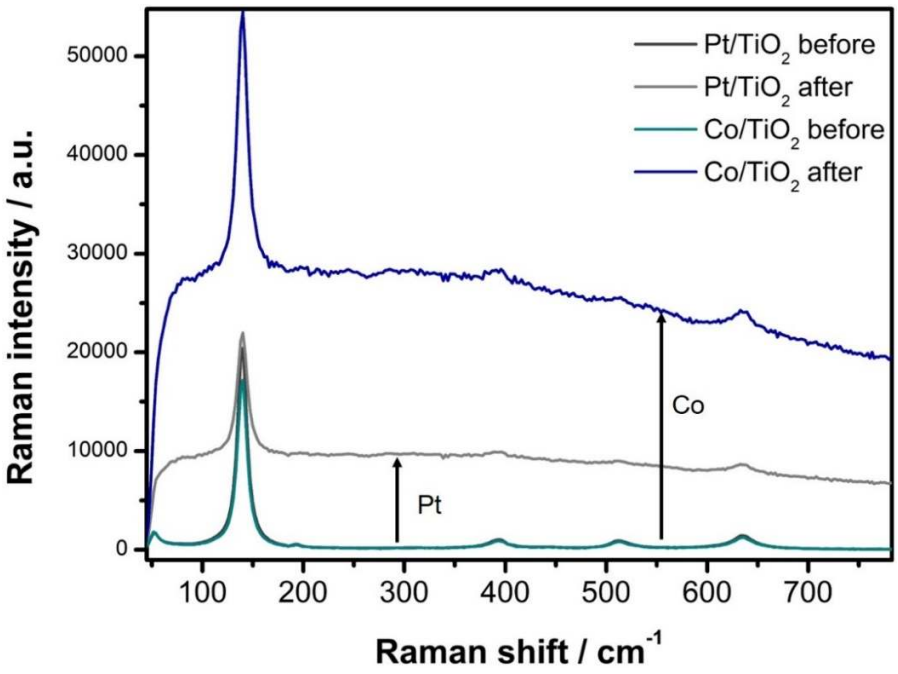

Figure S11. Raman spectra of Pt/TiO_2 and Co/TiO_2 (0.2 wt% of metal loading) before and after CO_2 photoreduction reaction with 785 nm excitation laser (red).

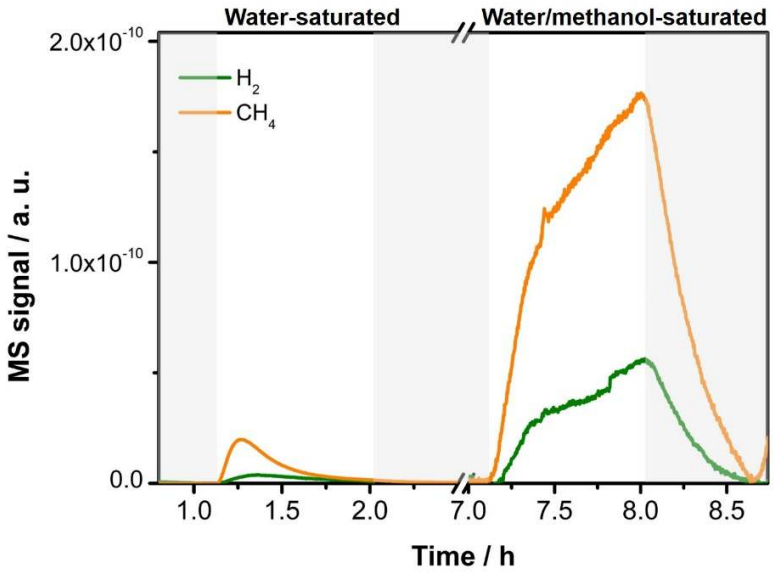

Figure S12. Concentration profiles (MS) of CH_4 (orange) and H_2 (green) during CO_2 photoreduction reaction over TiO_2. Two light off/on (grey region indicates light off) cycles were performed under the atmosphere of CO_2 saturated with **a**) water vapour and **b**) water/methanol vapour (10% v/v methanol).

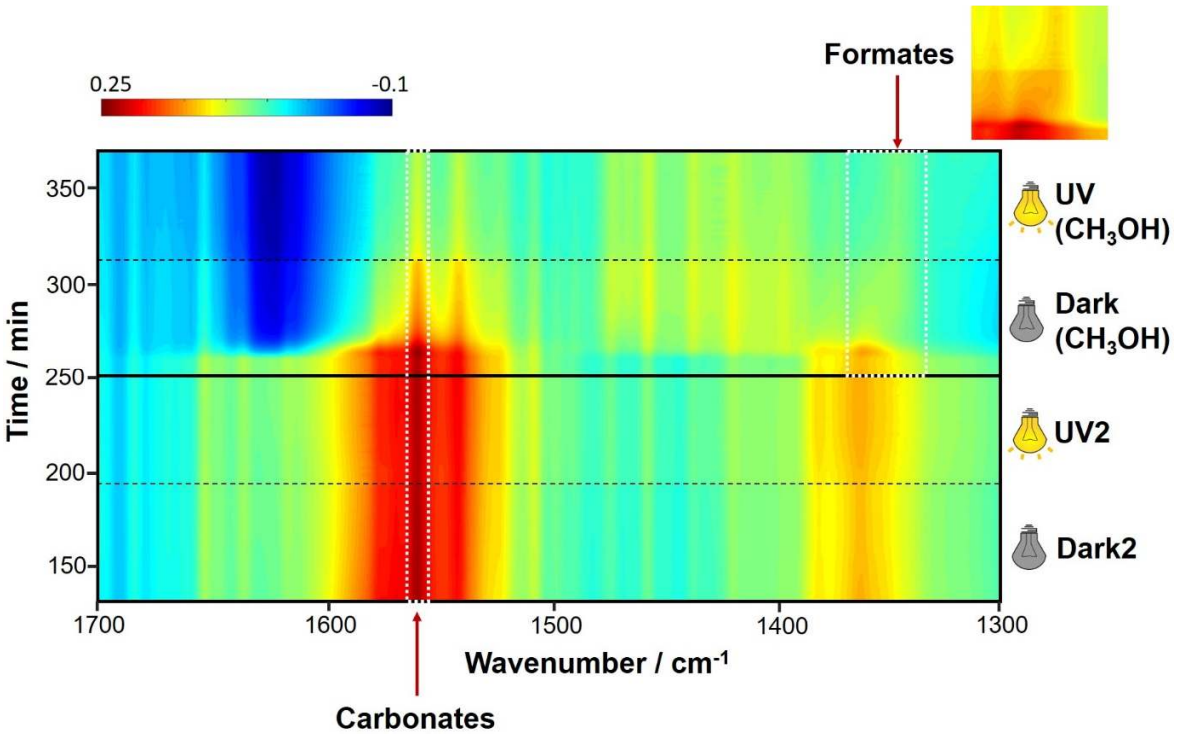

Figure S13. *In situ* DRIFT spectra during Dark2, UV2, Dark (CH_3OH), and UV (CH_3OH), from bottom to top, observed for bare TiO_2 during the CO_2 photoreduction reaction at 423 K. After two light off/on, an additional light

off/on cycles, photoreduction was evaluated by passing CO_2 saturated with water/methanol (10% v/v methanol).

Absorbance ranges from -0.1 (blue) to 0.25 (red).

REFERENCES

1. Monakhova, Y. B.; Astakhov, S. A.; Kraskov, A.; Mushtakova, S. P. Independent Components in Spectroscopic Analysis of Complex Mixtures. *Chemometr. Intell. Lab.* **2010**, *103*, 108-115.

2. Monakhova, Y. B.; Astakhov, S. A.; Mushtakova, S. P.; Gribov, L. A. Methods of the Decomposition of Spectra of Various Origin in the Analysis of Complex Mixtures. *J. Anal. Chem.*+ **2011**, *66*, 351-362.

3. Voronov, A.; Urakawa, A.; Beek, W. v.; Tsakoumis, N. E.; Emerich, H.; Rønning, M. Multivariate Curve Resolution Applied to in Situ X-ray Absorption Spectroscopy Data: An Efficient Tool for Data Processing and Analysis. *Anal. Chim. Acta.* **2014**, *840*, 20-27.